Role of the Hydrogen Bonds in Nitroanilines Aggregation: Charge Density Study of 2-Methyl-5-nitroaniline

Javier Ellena,[†,‡] Andrés E. Goeta,*[,§] Judith A. K. Howard,[§] and Graciela Punte[†]

IFLP & LANADI. Departamento de Física, Facultad de Ciencias Exactas, Universidad Nacional de La Plata, CC 67, (1900), La Plata, Argentina, and Instituto de Física de São Carlos, Departamento de Física e Informática, Universidade de São Paulo, C.P. 369, 13560, São Carlos (SP), Brazil, and Department of Chemistry, University of Durham, Durham, DH1 3LE, United Kingdom

Received: February 21, 2001; In Final Form: June 25, 2001

The electron charge distribution of 2-Methyl-5-nitroaniline has been studied from high-resolution single-crystal X-ray data at 100 K, and ab initio calculations which include X-ray structure factors computed from a superposition of ab initio molecular electron densities. Using the Hansen and Coppens' rigid pseudoatom multipolar model refinements were performed on both the experimental and the theoretical X-ray data sets from which, molecular atomic charges and dipolar moments were obtained. To understand the nature and the magnitude of the intermolecular interactions, the Atoms in Molecules theory was used to investigate the topology of the electron density of the in-crystal, both experimental interacting as well as theoretical noninteracting, and in-vacuum molecules. A meticulous analysis of the topological properties of the experimental charge density and of its Laplacian indicates, contrary to expectations, a two center character of the N−H···O synthons that induce the known polar chain formation in nitroanilines and the presence of a C_{methyl}-H···O interaction further strengthening the chains. It also shows the attractive nature of the rather strong C−H···O interactions that help the head-to-tail arrangement of the chains. They build two intermolecular six membered hydrogen bonded rings, embracing a N−H···O interaction, that originate centrosymmetric dimers which impair the macroscopic second harmonic generation of the title compound. The authenticity of a previously proposed closed shell C_{aryl}-H···π interaction between adjacent chains has been confirmed. The latter has not been observed in *m*-nitroaniline, 2-methyl-4-aniline or other related compounds with chains built from similar N−H···O synthons and assembled head-to-head. Crystallization causes a molecular electric dipolar moment higher than that of the free molecule, the latter being coincident with the experimental value in solution, and with the one calculated from the refinement of the theoretical X-ray data. It also induces changes in the charge density distribution and its topology, and an enhancement of the intramolecular conjugation that can be related to a molecular aggregation mechanism ruled by the N−H···O synthon. These findings strongly point to the existence of cooperative effects.

Introduction

The way in which molecules nucleate and organize in crystals remains an open question. Molecular aggregation and supramolecular ordering have been the subject of many studies, reviews, and revisions,[1] which were aimed at the understanding of the intermolecular interactions and the prediction of molecular assembling. In the case of organic compounds, discovering the nature and magnitude of those interactions and of their cooperative effects is crucial not only for the design of materials, but also to model biological systems. This knowledge would also help to understand the relationship between molecular and macroscopic properties in crystals. As part of the mentioned studies, experimental and theoretical research has been performed on the association of different nitroaniline derivatives.[2,3] The crystals of these compounds are especially interesting due to their potential nonlinear optical properties. The high second-order hyperpolarizabilities of many nitroaniline molecules have led to describe them as prototypes for second harmonic generation (SGH).[4]

It has been proposed that nitroaniline molecules assemble through weak and bifurcated hydrogen bonds (HBs) which induce polar chains development, apparently even in solution.[5] These chains might associate in a parallel or an antiparallel fashion. In the latter case, the macroscopic second harmonic generation is impaired. A way to obtain useful materials for SHG would be the use of molecules with large molecular hyperpolarizabilities and bearing functional groups capable of ruling the crystallization process through a noncentrosymmetric HB network.[6] Within this approach, nitroanilines, substituted nitroanilines, or similar compounds have been successfully used. However, it does not seem feasible at present to predict, in all cases, either the centric or the acentric character of the resulting assemblage,[7−9] or the relation between the molecular aggregation and the degree of conjugation of the free molecule. Besides, recent experimental[8,9] and theoretical findings on the amino geometry[10] and on hydrogen bond interactions,[11−13] coming from the currently available techniques, are showing that some of the commonly accepted models used to describe these systems might need to be improved. It can be mentioned, as examples,

* To whom correspondence should be addressed. E-mail: A.E.Goeta@durham.ac.uk.

† IFLP & LANADI. Departamento de Física, Facultad de Ciencias Exactas, Universidad Nacional de La Plata.

‡ Instituto de Física de São Carlos, Departamento de Física e Informática, Universidade de São Paulo.

§ Department of Chemistry, University of Durham.

10.1021/jp010688h CCC: $20.00 © 2001 American Chemical Society
Published on Web 08/29/2001

the recent X-ray Compton effect study performed on ice I*h*,[11] which would indicate that charge is built up in some HBs traditionally accepted as ionic and the indications, coming from Gatti et al. calculations[12] on urea, on the possibility that π conjugation propagates through HBs. These results might imply the necessity for a revision of the oriented molecular gas model, which had been used to analyze the nonlinear optical properties of molecular crystals.

We have studied the geometry and molecular packing patterns of several aniline and nitrobenzene derivatives.[14] They included substitutions showing different degree of conjugation and capacity to establish HBs. Our investigation, along with some results of theoretical calculations existing in the literature[2], showed the lack of reliable experimental data to establish the interplay between intramolecular charge transfer, supramolecular assembly, and nonlinear optical phenomena in nitroaniline crystals.

On the basis of Bader's atoms in molecules (AIM) theory,[15] the nature of chemical bonds and intermolecular interactions in a given system can be disclosed analyzing the topology of the charge density of representative compounds. The examination of the crystalline electron density is an appropriate tool to study the influence of the crystal environment and the intermolecular interactions on the molecular physical properties. From a previous room-temperature single crystal study[7] we knew that 2-methyl-5-nitroaniline crystallizes in a centrosymmetric space group. However, it presents an HB's scheme, confirmed by a recent neutron diffraction study,[8] similar, on geometrical grounds, to that of its noncentric and highly conjugated isomer, 2-methyl-4-nitroaniline (2M4NA). The latter has been studied in detail due to its exceptionally large electrooptical[16] and SHG[17] coefficients. A charge density analysis of 2M4NA had been performed[18] but data were not good enough to produce convincing conclusions on the nature of the intermolecular interactions. Besides, the possibility of obtaining interaction densities from accurate X-ray diffraction data of acentric crystals seems to be a matter of controversy at present[3,19,20]. Recently, Coppens and collaborators have carried out extensive theoretical and experimental studies of the centrosymmetric *p*-nitroaniline[3] but they have constrained the molecular geometry. In particular, the amino group was assumed to be planar[3b]. We know from our own neutron diffraction studies[8,9] and from ab initio calculations[10,14] that the amino group is not necessarily planar. Therefore, a geometrically unconstrained charge density study of 2-methyl-5-nitroaniline (2M5NA) seems suitable to retrieve valuable information on the validity of the bifurcated HB model to describe nitroanilines organization in polar chains, and on the relationship between intramolecular conjugation and HB formation.

The net redistribution of the molecular charge density originated by the presence of hydrogen bonds, and the possible existence of cooperative effects, cannot be deduced only from experimental data because the charge distribution of the free molecule cannot be obtained from X-ray diffraction. A study of the redistribution of the molecular charge density necessarily involves a systematic comparison of experimental data with that obtained from theoretical calculations. Therefore, ab initio calculations were performed to study the free molecule and to simulate X-ray diffraction data and the results were compared with the experimental ones.

Experimental Data

Data Collection and Reduction. An orange single crystal with dimensions 0.2 × 0.34 × 0.44 mm^3 was used to collect data at 100K over a period of 10 days using a Siemens SMART CCD system equipped with an Oxford Cryosytems N_2 open flow cryostat.[21] To reduce $\lambda/2$ contamination effects,[22] because CCD area detectors have no energy discrimination, reflection data were measured using Mo−Kα radiation with X-ray generator settings of 35kV and 55mA. A complete sphere of data was collected twice, one after another, with the detector centered at 29° in 2θ and at a distance of 4.5 cm from the crystal. Runs consisting of series of narrow ω-scans (0.2°) at ϕ settings of 0°, 90°, 180°, 270°, 45°, 135°, 225°, and 315° were performed to collect a total of 6660 frames (20s per frame) containing data up to $2\theta_{max} = 60.65°$. Following this and in the same way, another 6653 frames were collected using an exposure time of 40s per frame with the detector centered at $2\theta = 68°$. The increase in the exposure time of the latter set of frames aims at increasing the accuracy of the measurement, compensating for the decay in the intensity of the reflections at high values of 2θ. In this way, reflections were collected up to a resolution of $\sin\theta/\lambda \leq 1.043$ Å^{-1} ($2\theta_{max} = 95.68°$ using Mo−Kα). The information about the valence electron distribution, the one we are interested in, is carried by the low angle reflections. Then, to improve our measurements in this region of the reciprocal space, another 7470 20s frames were collected again at $2\theta = 29°$ with ϕ settings of 22.5°, 112.5°, 202.5°, 292.5°, 67.5°, 157.5°, 247.5°, 337.5°, 10°, and 100°. In this way, the reciprocal sphere until $2\theta = 60°$ was collected about four times, in different azimuthal positions. We believe that this approach allows us to increase the accuracy of the measured intensities needed for a charge density study.

TABLE 1: Crystallographic Data

parameter	X-ray	neutron
space group	$P2_1/n$	$P2_1/n$
temperature (K)	100(1)	100(1)
λ(Å)	0.71073	0.5−5
a(Å)	9.373(2)	9.369(2)
b(Å)	5.562(1)	5.563(1)
c(Å)	13.645(3)	13.626(3)
β(°)	92.54(3)	92.36(3)
V(Å^3)	711.5(3)	709.6(3)
Z	4	4
measured reflections	71734	17278
unique reflections	6746	3386
R_{int}	0.0286	0.06
observed reflections ($I > 2\sigma(I)$)	4147	3386
absorption correction	Yes	Yes
number of parameters	368	172
R(F)	1.32	6.69
R_{all}(F)	4.61	6.69
*w*R(F)	1.65	
*w*R(F^2)	3.22	15.44

Crystal data, including for comparison the parameters obtained in the neutron diffraction experiment,[8] are detailed in Table 1. Data collection and unit cell determination and refinement were carried out using the SMART software.[23] Raw frame data were integrated using the SAINT program.[24] Unit cell parameters are normally calculated after data integration by the SAINT software. It gives statistically correct but yet meaninglessly small standard uncertainties based on a very large number of reflections. Instead, the unit cell reported in Table 1 was calculated from multiple measurements and standard uncertainties calculated from the spread of these measurements. The different unit cell measurements were performed by "thresholding" all the collected frames in groups of 4 consecutive runs (basically one reciprocal sphere) and choosing the reflections that fulfilled a set criteria: $26° \leq 2\theta \leq 56°$ and $I/\sigma(I) \geq 90$ for the low angle runs; $46° \leq 2\theta \leq 76°$ and $I/\sigma(I)$

≥ 70 for the high angle runs. Each unit cell measurement was carried out from the centroid values of approximately 440 reflections.

An incident beam correction was performed to the data using the program SADABS[25] followed by a Gaussian face-indexed absorption correction using the program XPREP.[26] Data were then merged using the program SORTAV.[27] The analysis of the data using this same program showed that from the 69074 reflections collected, 66043 measurements were space group allowed giving 6746 unique reflections. From these, 40 were measured only once, 312 twice, and 6394 three times or more. From the 66043 measurements, 637 were rejected as outliers affecting 230 means. Only 17 space group allowed reflections were unmeasured below the maximum resolution reached.

Multipole Refinement. To take into account the residual bonding density not modeled by a conventional spherical refinement,[14] a multipolar refinement[28] was performed using the Hansen and Coppens model[29] incorporated in the XD package.[30] Radial Slater type functions with standard ζ-values[31] were applied and multipoles up to $l_{max} = 3$ (octupoles) for non-H atoms and $l_{max} = 2$ (quadrupoles) for H atoms were used. The addition of hexadecapoles to non-H atoms did not improve the model. A different set of contraction−expansion coefficients was refined for each chemically different atom. Then, a set of κ and κ' coefficients was refined for each O and N atom. A common set of κ and κ' coefficients was used for the aromatic carbon atoms and a different one for the methyl carbon. For each H atom, a different κ coefficient was refined. After Hehre et al.[32] the κ' coefficients of the H atoms were fixed at 1.24 to take into account the atoms contraction. No chemical or symmetry restraints were applied during the refinement. The application of an extinction correction proved to be unnecessary.

The multipolar refinement was performed on F. Positions and thermal parameters of the hydrogen atoms were fixed at the neutron refinement values[8] and all the other atomic parameters were allowed to refine freely. The function minimized was the following: $\Sigma_{\mathbf{H}}\ w_{\mathbf{H}}(|F_{obs}(\mathbf{H})| - k|F_{cal}(\mathbf{H})|)^2$. The weighting scheme used was $w_{\mathbf{H}} = (\sigma^2(F_{obs}(\mathbf{H})) - 0.07(F_{obs}2(\mathbf{H})))^{-1}$, the second term in the weighting scheme was introduced to take into account any systematic errors originated in the equipment. The structure factors for the neutral atoms were obtained from the *International Tables for X-ray Crystallography* (1974, Vol. IV). 4147 reflections with $I > 2\sigma(I)$ were used in the refinement. The figures of merit obtained are shown in Table 1. Table 1S and Table 2S give the atomic positions and thermal parameters, respectively. Intramolecular bond distances and angles are given in Table 3S, whereas Figure 1 shows the molecule under study, together with the labeling scheme and intermolecular contacts discussed below.

According to Hirshfeld,[33] the mean square displacement amplitude (MSDA) for bonded atoms along the bond vector in organic molecules should be almost identical. Therefore, for well-refined structures, on the basis of good data sets, the MSDA differences should be, and usually are, lower than 10×10^{-4} Å^2. Nevertheless, they can be very different along the other directions. Internal libration of the NO_2 group bound to an aromatic ring has been described in the literature.[34] In some cases of room-temperature measurements, the amplitude of the libration had been so large that the structure had to be refined using a static or occupational disordered model.[35] In the present study, only one of the oxygen atoms presents MSDA values that exceed the above-mentioned limit. The average MSDA differences (Table 4S) for pairs of bonded atoms is 2.3×10^{-4} Å^2. Therefore, the final model can be considered consistent with the rigid-bond hypothesis.

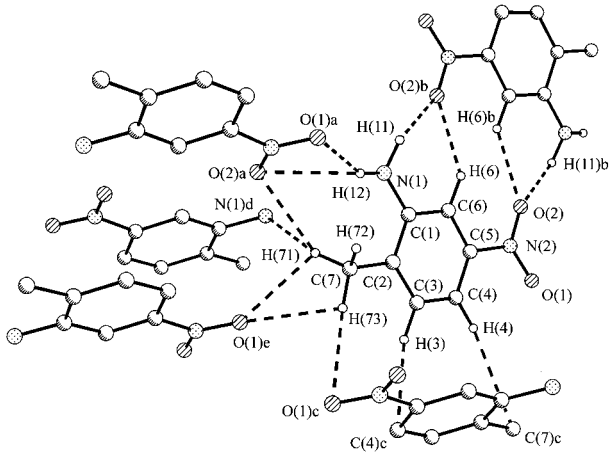

Figure 1. View of the title compound showing the labeling scheme. Intermolecular contacts discussed in the text are indicated by dash lines. H-atoms not belonging to the central molecule have been omitted for clarity.

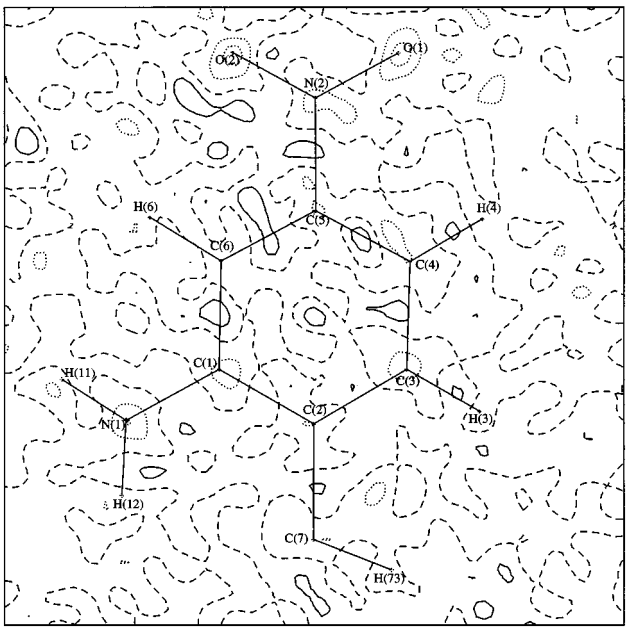

Figure 2. Residual density map in the mean molecular plane obtained in the final cycle of the multipole refinement. Contours at 0.05 e.Å^{-3} intervals. Solid contours positive, dashed contour zero and dot contours negative.

A residual density map in the molecular plane obtained in the final cycle of refinement (see Figure 2) indicates the good quality of the final model. The minimum and maximum values found for the residual density were −0.128 and 0.095 e/Å^3, respectively. The root-Mean-Square of the map was 0.026e/Å^3. Furthermore, the random distribution of peaks and hollows in this map shows that the obtained model takes account of the deformation density. Final refined values for the expansion-contraction coefficients (κ & κ') and monopolar population parameters are shown in Table 2, whereas full multipolar population values have been deposited as Table 5S.

Theoretical Data

Free Molecule. The free molecule wave functions were calculated with the *GAUSSIAN94* program package.[36] Geometry optimization was carried out applying the analytical gradient

TABLE 2: Expansion-Contraction Coefficients and Monopoles' Population Parameters from the Multipolar Refinement of Experimental and Theoretical Structure Factors (^{T})

atom	O(1)	O(2)	N(1)	N(2)	C(1)	C(2)	C(3)	C(4)	C(5)	C(6)	C(7)
κ	0.986(1)	0.978(1)	0.980(1)	0.975(1)			0.988(1)				0.984(1)
κ^{T}	0.984(1)	0.983(1)	0.988(1)	0.970(1)			0.983(1)				1.010(1)
κ'	1.017(9)	1.183(8)	0.866(6)	0.797(3)			0.902(2)				0.961(5)
κ'^{T}	1.049(4)	1.033(4)	0.902(4)	0.797(2)			0.904(1)				0.968(4)
P_v	6.14(3)	6.23(3)	5.14(8)	5.16(4)	4.07(3)	4.05(2)	4.08(3)	4.06(3)	3.99(3)	4.10(3)	4.14(11)
P_v^{T}	6.14(1)	6.14(1)	4.98(2)	5.12(1)	4.02(1)	4.09(1)	3.99(1)	4.02(1)	3.96(1)	3.99(1)	3.62(3)

atom	H(11)	H(12)	H(3)	H(4)	H(6)	H(71)	H(72)	H(73)
κ	1.189(7)	1.244(7)	1.151(5)	1.249(6)	1.240(6)	1.189(7)	1.175(6)	1.222(7)
κ^{T}	1.141(3)	1.141(3)	1.154(3)	1.180(3)	1.155(3)	1.113(3)	1.120(3)	1.131(3)
κ'				1.24				
P_v	0.86(5)	0.74(5)	0.94(4)	0.78(4)	0.78(4)	0.91(5)	0.95(6)	0.87(5)
P_v **T**	0.96(1)	0.96(1)	0.97(1)	0.88(1)	0.93(1)	1.10(1)	1.09(1)	1.06(1)

method.[37] Atomic coordinates from a neutron diffraction experiment[8] were used for the initial conformation. The molecular geometry full optimization was performed using a 6-31G* basis set,[38] employing as convergence criterion the default threshold limits for both, the maximum force and the displacement. Sim and collaborators[39] have shown the importance of the inclusion of the electron correlation effects in the determination not only of the equilibrium geometry but also of the nonlinear optical properties of nitroanilines. They found that the MP2 level of theory gave a better description of the electron density of the fundamental state than the RHF level. They also found that the MP2 results agreed with the ones reached from higher levels of theory and with experimental values in gas phase. Therefore, the MP2 level of theory was employed in the optimization process. The optimized geometry was confirmed as minimum by frequency calculation. Use of a larger basis set (6-31G**, 6-311G**) did not show appreciable differences neither in geometry nor in charge density topology.[14]

Periodic HF Calculations. Periodic Hartree−Fock calculations were performed with the CRYSTAL98 program.[40] Using the keyword MOLSPLIT available in this program, the electronic wave function was calculated for a superposition of molecular densities arranged in the same geometry as in the crystal. Cell data and fractional coordinates for the calculation were those resulting from the multipole refinement described above (Tables 1 and 1S, respectively). In these calculations, a 6-31G** basis set,[38] which has been successfully used for periodic calculations in other systems[3a,12,41], was employed. 4147 theoretical structure factors, the same ones used for the multipole refinement of the experimental data, were then calculated directly from CRYSTAL98. These structure factors were employed to perform a multipole refinement on F with the XD package,[30] in the same way as for the experimental data. No atomic temperature refinement was performed and all positional parameters were fixed. Following Spackman and collaborators[19], thermal effects on high-angle data were simulated by multiplying each structure factor by the weight $\exp[-4(\sin\theta/\lambda)^2]$. This is equivalent to using an overall isotropic temperature factor $B = 2.0$ Å^2. The multipole population parameters obtained have been deposited as Table 6S. Selected values are included in Table 2 for comparison.

Results and Discussion

Solid State Charge Density. The electrostatic properties of the molecular electron density distribution of 2M5NA were obtained using the program XDPROP implemented in the XD program package.[30] The molecular electric dipole moment in the crystal is almost coplanar with the aromatic ring and has the expected direction: from the negative charged NO_2 group to the middle point between the positive charged NH_2 and CH_3 groups. Its value, 10.6(9)D, is higher than the experimental value

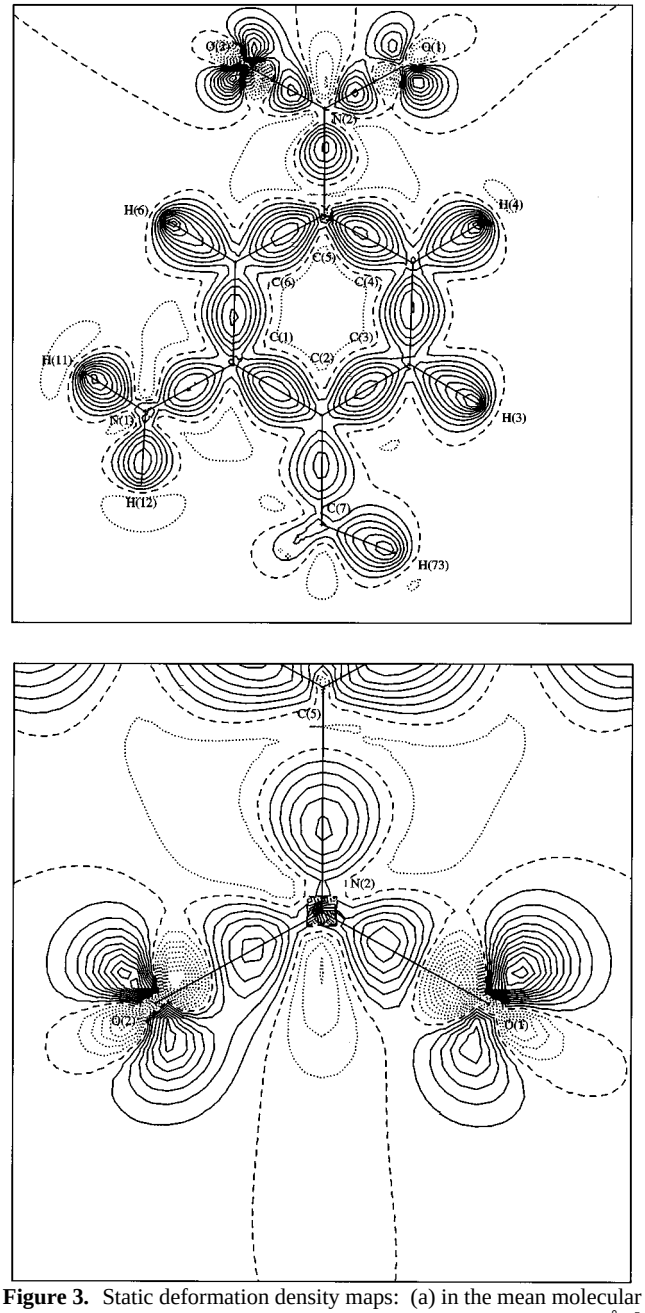

Figure 3. Static deformation density maps: (a) in the mean molecular plane, (b) in the plane of the nitro group. Contour levels at 0.1 e.Å^{-3} intervals. Solid contours positive, dashed contour zero and dot contours negative.

TABLE 3: Intramolecular Bond Critical Points[a] and Their Properties[b]

bond	ρ(r)	$\nabla^2\rho$(r)	D1	D2	λ_1	λ_2	λ_3	ϵ
O(1)−N(2)	3.346(24)	−9.992(65)	0.6193	0.6094	−29.81	−25.50	45.32	0.17
	3.317(8)	−12.310(22)	0.6068	0.6218	−28.25	−26.47	42.41	0.07
	2.87	−9.27	0.641	0.602				0.06
O(2)−N(2)	3.434(26)	−16.229(72)	0.6457	0.5821	−32.02	−27.69	43.48	0.16
	3.321(7)	−12.213(21)	0.6078	0.6200	−28.47	−26.54	42.80	0.07
	2.86	−9.23	0.642	0.602				0.06
N(1)−C(1)	2.185(16)	−20.503(48)	0.7964	0.5810	−17.45	−14.54	11.49	0.20
	2.144(5)	−21.523(16)	0.8002	0.5772	−17.23	−14.83	10.53	0.16
	1.88	−16.84	0.829	0.569				0.05
N(1)−H(11)	2.407(74)	−36.844(450)	0.7186	0.2827	−31.95	−30.25	25.36	0.06
	2.360(19)	−32.410(114)	0.7145	0.2869	−30.36	−27.65	25.60	0.10
	2.12	−32.90	0.736	0.278				0.05
N(1)−H(12)	2.280(65)	−30.520(414)	0.7289	0.2735	−30.66	−28.09	28.23	0.09
	2.341(18)	−31.747(108)	0.7143	0.2880	−30.08	−27.24	25.57	0.10
	2.12	−32.90	0.737	0.278				0.05
N(2)−C(5)	1.717(13)	−13.889(46)	0.9055	0.5579	−12.22	−10.02	8.35	0.22
	1.756(5)	−16.365(20)	0.9424	0.5210	−12.11	−10.67	6.41	0.14
	1.60	−10.51	0.879	0.589				0.05
C(1)−C(2)	2.101(13)	−18.842(36)	0.7216	0.6985	−16.02	−12.75	9.93	0.26
	2.087(4)	−19.419(10)	0.7300	0.6902	−15.92	−12.79	9.30	0.24
C(1)−C(6)	2.079(13)	−18.639(35)	0.7169	0.6879	−15.60	−12.57	9.53	0.24
	2.120(4)	−19.869(11)	0.7233	0.6814	−16.16	−12.83	9.12	0.26
C(2)−C(3)	2.122(14)	−18.912(36)	0.6977	0.6992	−16.10	−12.54	9.73	0.28
	2.134(4)	−19.741(11)	0.7048	0.6920	−16.22	−12.72	9.20	0.27
C(2)−C(7)	1.683(17)	−11.341(36)	0.7638	0.7386	−11.10	−10.50	10.26	0.06
	1.723(5)	−11.996(12)	0.7752	0.7271	−11.78	−11.06	10.85	0.07
C(3)−C(4)	2.086(15)	−18.758(37)	0.6797	0.7167	−15.49	−12.64	9.37	0.22
	2.134(4)	−19.924(11)	0.6929	0.7034	−16.03	−13.04	9.15	0.23
C(4)−C(5)	2.187(15)	−21.230(40)	0.6490	0.7412	−16.83	−13.33	8.93	0.26
	2.166(4)	−20.979(11)	0.6534	0.7367	−16.49	−13.10	8.61	0.26
C(5)−C(6)	2.147(14)	−19.872(37)	0.7231	0.6679	−16.46	−12.78	9.37	0.29
	2.158(4)	−20.611(11)	0.7296	0.6614	−16.48	−12.92	8.79	0.28
C(3)−H(3)	1.917(45)	−20.824(187)	0.6977	0.3858	−17.95	−17.19	14.31	0.04
	1.924(13)	−21.437(49)	0.6744	0.4091	−17.56	−16.81	12.93	0.04
C(4)−H(4)	1.895(45)	−20.368(186)	0.6985	0.3877	−18.27	−17.23	15.14	0.06
	1.915(13)	−20.948(53)	0.6946	0.3916	−17.89	−17.13	14.07	0.04
C(6)−H(6)	1.912(45)	−20.646(197)	0.7096	0.3719	−18.78	−17.75	15.89	0.06
	1.936(13)	−21.703(51)	0.6848	0.3966	−17.96	−17.08	13.33	0.05
C(7)−H(71)	1.924(55)	−20.437(223)	0.7025	0.3852	−18.02	−17.69	15.27	0.02
	1.882(12)	−19.817(41)	0.6577	0.4299	−16.52	−16.00	12.70	0.03
C(7)−H(72)	1.841(63)	−18.857(235)	0.6857	0.4090	−16.75	−15.83	13.72	0.06
	1.830(13)	−18.058(44)	0.6672	0.4271	−15.89	−15.51	13.34	0.02
C(7)−H(73)	1.863(56)	−18.607(219)	0.6902	0.3950	−17.29	−16.54	15.22	0.05
	1.887(13)	−19.521(44)	0.6619	0.4232	−16.66	−16.28	13.42	0.02

[a] First row: from experimental data, second row: from theoretical structure factors of noninteracting molecules, third row: from ab initio free molecule calculation at the MP2/6-31G* level. [b] The electron density ρ (e Å^{-3}), its Laplacian $\nabla^2\rho$ (e Å^{-5}) and the curvatures $\lambda_{1,2,3}$ (e Å^{-5}) are the values at the BCPs. D1 & D2 are the distances from the first and second atom respectively to the bond CP and ϵ is the bond ellipcity.

in a solution of benzene, 6.12(5)D.[42] This enhancement of the dipole moment agrees with findings in 2M4NA,[18] in which the value increases from 8.2 D for the free molecule[43] to 25(8)D[18] for the molecule in the solid state. Molecular dipole enlargement in solids is accepted at present[3,12,19,41,44] despite some results which are contradictory, see for example the recent experimental charge density study on urea crystals.[45] From simulated X-ray diffraction data, and in coincidence with theoretical calculations on supramolecular aggregates,[12,41] Spackman et al.[19] found considerable enhancement of the molecular dipolar moment in hydrogen bonded crystals. On the basis of experimental results assisted by theoretical calculations, Feil[46] concluded that hydrogen bonds in hydrated oxalic acid reinforce the polarity of the molecules that participate in the bond. Besides, he found that charge transfer is small. On the same grounds that Feil does, Zhang and Coppens[47] interpreted the increase in dipole moment, in systems with HBs of different strengths, as a quantitative measure of the environment's polarizing field.

Figure 3a shows a static deformation density map of the molecular charge density on the mean plane of the aromatic ring. This map was generated in direct space using the multipolar populations of one molecule. As expected, positive deformation density is observed in all bonds. Figure 3b shows a static deformation density on the plane of the nitro group. Differences in the oxygen lone pairs heights and positions can be seen from this figure. Differences are also observed when comparing both N−O and N−H bonds. All these differences are believed to be due to different environments, i.e., different intermolecular interactions according with Spackman et al.[19]

To make a quantitative analysis of these observations the molecular chemical bonds' topology was investigated. An evaluation of the (3,−1) bond critical points (BCPs) of the charge density, ρ(r), was performed. Table 3 lists the bond critical points, the values of the charge density, ρ(r), the Laplacian, $\nabla^2\rho$(r), the eigenvalues of the Hessian, bonds' ellipticity, ϵ, at the BCPs and the distances from the BCPs to the bound atoms. The values of ρ(r), $\nabla^2\rho$(r) and ϵ in the BCPs of C−C bonds in the aromatic ring are within the expectations.[3,48] The ellipticity values found in the N(1)−C(1), N(2)−C(5), O(1)−N(2), and O(2)−N(2) BCPs show the partially double character of these bonds. The observed shift of the BCPs from the bonds' midpoints in C(1)−N(1), C(5)−N(2), and

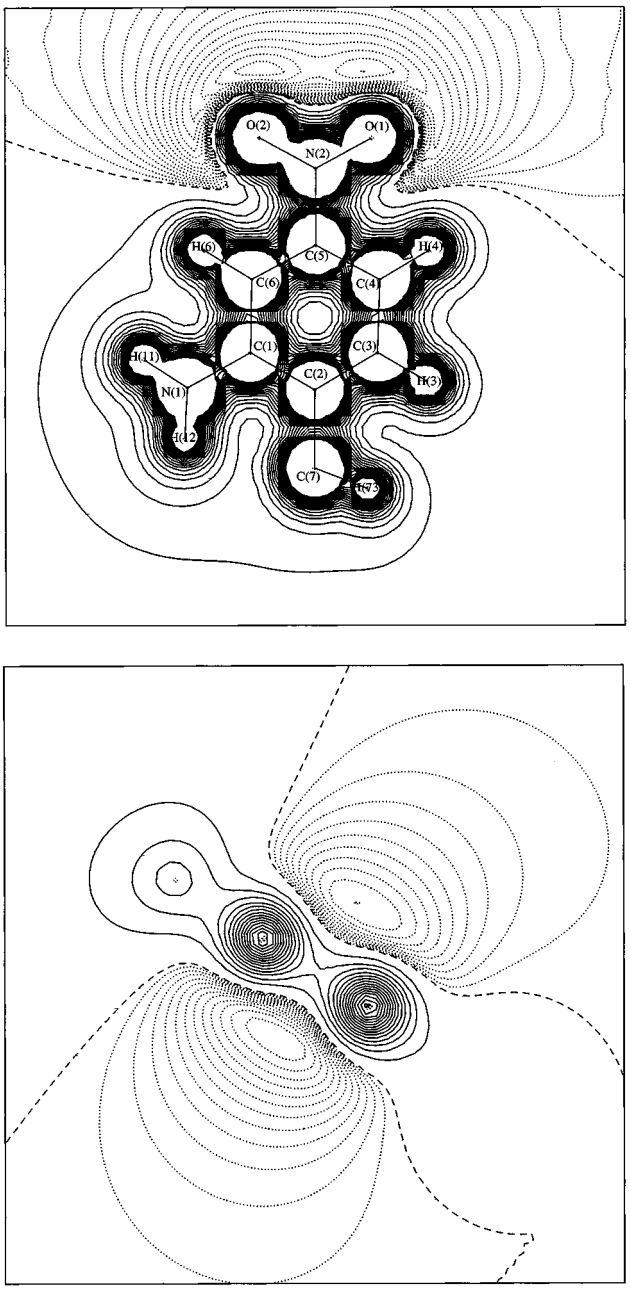

Figure 4. Contour maps of the electrostatic potential. (a) In the mean molecular plane, (b) in a plane perpendicular to the mean molecular plane and perpendicular to the C(1)−C(6) and C(3)−C(4) bonds. Negative contours levels at 0.01 e.Å^{-1} intervals and positive contours levels at 0.1 e.Å^{-1} intervals. Solid contours positive, dashed contour zero and dot contours negative.

O(2)−N(2) and in all C−H bonds indicates polarization. Other features of the experimental in-crystal charge density topology are compared with the theoretical ones and discussed in depth below.

To get a better insight into the electrostatic properties of the molecules of 2M5NA the molecular electrostatic potential was calculated using the Su and Coppens method.[49] The contribution to the electrostatic potential was determined using the exact form for all multipoles ($l_{max} = 3$). Figure 4a shows the molecular electrostatic potential on the mean molecular plane. It can be seen that the negative isocontours are concentrated around the nitro group. The value of the molecular electrostatic potential at the global minimum, which is located close to O(2) and off the mean aromatic ring plane on the same side where the aminic hydrogen atoms are, is −0.20 e/Å. There is a local minimum, of −0.16 e/Å, close to O(1), and on the mean molecular plane. Figure 4b shows the molecular electrostatic potential on a plane perpendicular to the mean aromatic ring plane and perpendicular to the bonds C(1)−C(6) and C(3)−C(4). It can be seen from this figure, that two regions of negative electrostatic potential are located at both sides of the aromatic ring, on planes parallel to its mean plane. The local minima in these two regions are −0.10 and −0.13 e/Å, located at the ring center off the mean aromatic ring plane toward both sides. The deeper minimum of these two is located on the side opposite to that where the global minimum is.

Intermolecular Interactions. The hydrogen bond pattern, according to neutron diffraction results[8] shows one of the aminic hydrogen atoms connected, through a bifurcated HB, with the two oxygen atoms of a nitro group, related by the symmetry operation (a): $^1/_2 + x$, $^1/_2 - y$, $z - ^1/_2$. This was in accordance with findings of Panunto et al..[5] These N−H...O_{nitro} interactions link molecules related by a glide plane and induce the formation of infinite polar chains along [10$\bar{1}$]. Molecules in the chain are additionally linked by a weak C_{methyl}-H···O interaction, which is depicted in Figure 1. Intermolecular distances also suggest that the molecules related by an inversion center, (b): $2 - x$, $1 - y$, $1 - z$, are linked by four HBs (see Figure 1). This causes the generation of centrosymmetric dimers. Two of the mentioned HBs involve the amino hydrogen H(11) and the oxygen O(2). The other two HBs, connect the aromatic hydrogen H6 with the same oxygen. This means, according to Bernstein et al.,[50] that two intermolecular six membered HB rings are linking two aromatic systems. Therefore, some degree of resonance can be assumed which further stabilizes the dimeric units.[51] So, by combining the interactions described above, two adjacent antiparallel chains are alternately joined by centrosymmetric dimer interactions. This gives rise to nonpolar ribbons that inhibit the macroscopic second-order nonlinear optical response of 2M5NA. Table 7S gives all the geometrical details of the intramolecular and intermolecular contacts that can be interpreted as hydrogen bonds on geometrical grounds.

To confirm the existence of these interactions and enlighten their nature, the topology of the experimental charge density in the intermolecular region was investigated. The existence of bond paths between the involved atoms was examined and a search for the (3,−1) BCPs along the paths was performed. Results are shown in Table 4. According to Bader[15,52] the presence of a bond path linking two atoms guarantees the existence of an attractive interaction. In particular atoms joined by closed shell interactions, like hydrogen bonds, should be connected by a bond path characterized by the existence of a (3,−1) BCP at which $\rho(\mathbf{r_C})$ should be small and $\nabla^2\rho(\mathbf{r_C})$ positive. The meticulous examination performed, showed the existence of a bond path and the corresponding (3,−1) BCP between H(12) and O(1)a. No path was found between H(12) and O(2)a. The complete analysis of the interactions that stabilize the chains lead to find a bond path and (3,−1) BCP between H(71) and O(2)a (Figure 5a). The analysis of the bond paths between the atoms that build the centrosymmetric dimers supports the existence of attractive interactions. Corresponding (3,+1) ring critical points were found for the two intermolecular six-membered HB rings linking the two aromatic systems (Figure 5b). A (3,−1) critical point was found to confirm the presence of a close shell interaction between the aromatic hydrogen H(3) and the benzene ring of a molecule in a neighbor chain. Moreover, the H atom points toward the π cloud on the side of the aromatic ring where the most negative region of the

TABLE 4: Experimental Geometrical and Topological Parameters of the Critical Points for Hydrogen Bonds

D − H... A	D − H... A (°)	H...A (Å)	D_1 (Å)	D_2 (Å)	Bond Path Length (Å)	ρ(r) (e/Å^3)	$\nabla^2\rho$(r) (e/Å^5)	λ_1	λ_2	λ_3	ϵ
Within the chains:											
N(1) − H(12)...O(1)a	153.83(2)	2.2228(4)	0.8377	1.4008	2.2424	0.065(12)	1.069(18)	−0.35	−0.27	1.69	0.32
N(1) − H(12)...O(2)a	142.28(2)	2.7436(4)	no critical point found								
C(7) − H(71)...O(2)a	128.56(2)	2.7521(6)	1.1838	1.5718	2.7629	0.030(6)	0.444(2)	−0.11	−0.08	0.63	0.37
Dimer interaction:											
N(1) − H(11)...O(2)b	145.48(2)	2.3180(4)	0.9333	1.4214	2.3702	0.066(10)	0.655(12)	−0.33	−0.29	1.28	0.15
C(6) − H(6)...O(2)b	142.05(2)	2.3503(4)	0.9377	1.4132	2.3626	0.061(10)	0.991(9)	−0.26	−0.20	1.45	0.30
Others:											
C(7) − H(73)...O(1)c	154.34(2)	2.9573(6)	1.2557	1.7529	3.0701	0.024(4)	0.284(2)	−0.07	−0.04	0.40	0.53
C(3) − H(3)...C(4)c	160.29(1)	2.6473(2)	1.0411	1.6472	2.9094	0.062(7)	0.597(5)	−0.19	−0.09	0.87	1.20
C(4) − H(4)...C(7)c	142.45(1)	3.0109(4)	1.1951	1.8298	3.2950	0.026(6)	0.382(2)	−0.08	−0.02	0.48	3.34
C(7) − H(71)...N(1)d	151.12(2)	2.7610(3)	1.1433	1.6248	2.7776	0.037(6)	0.467(4)	−0.16	−0.13	0.75	0.19
C(7) − H(71)...O(1)e	109.47(2)	2.7239(4)	no critical point found								
C(7) − H(73)...O(1)e	105.71(2)	2.7862(4)	no critical point found								
Intramolecular:											
C4 − H4...O1	94.24(2)	2.4203(4)	no critical point found								
C6 − H6...O2	95.16(1)	2.3969(4)	no critical point found								

[a] Symmetry operations: a: 1/2+*x*, 1/2−*y*, *z*−1/2; b: 2−*x*, 1−*y*, 1−*z*; c: 3/2−*x*, *y*−1/2,1/2−*z*; d: 5/2−*x*, *y*−1/2, 1/2−*z*; e: 1/2+*x*, −1/2−*y*,*z*−1/2.

electrostatic potential, between the two at both sides of the aromatic ring, is found. The analysis of the bond path, Figure 5c, shows that it goes from H(3) to the midpoint of the aromatic C(3)c−C(4)c bond and then bends sharply toward C(4)c. This result is consistent with other experimental results[53] and with theoretical calculations.[54] Rozas et al.[54a] have shown that X−H...π interactions, where the π system may be a C−C benzene bond, are weak hydrogen bonds, whereas Tang and Cui[54b] when studying X−H... π hydrogen bonded complexes, from ab initio calculations, obtained a bond path shape similar to our experimental one. According to a theoretical study of C−H... π complexes by Novoa and Mota,[54c] when the complex shows a high symmetry the bond path connects the C−H hydrogen with the center of the C−C bond or the middle of the ring. A slight distortion of that highly symmetric conformation switches the connection to one of the atoms of the π system. Therefore, in the present case the C(3)−H(3)...C(4)c contact can be interpreted as a C−H...π interaction. The molecules connected by this interaction are also linked by bond paths between C(7)−H(73)....O(1)c and C(4)−H(4)...C(7)c (see Table 4). The topology of the (3,−1) CPs found and the bond paths shown in Figure 5c, seem to endorse the closed shell character of these interactions. It could be said that in principle the C(4)−H(4)....C(7)c "interaction" does not make chemical sense. The bond path goes from H(4) to the midpoint of the C(7)c−H(72)c bond and then bends sharply toward C(7)c. This would support an intermolecular interaction of the kind C(4)−H(4)...σ (σ = sigma bond), similar to N−H...σ interactions observed before in several boraneamines.[55] These compounds present what is called a dihydrogen bond, N−H$^{\delta+}$...$^{\delta-}$H−B, which has been studied by neutron diffraction[55] and theoretical calculations.[56] The geometrical features of this dihydrogen bond are strikingly similar to the C(4)−H(4)...H(72)c−C(7)c ones. The H(4)...H(72) distance (2.376 Å), though shorter than the sum of the van der Waals radii for two hydrogen atoms (2.4 Å), is longer than the equivalent distances in the referred boraneamines (by at least 0.2 Å). This would be expected on the basis that the electrostatic interaction between H$^{\delta+}$...$^{\delta-}$H in the title compound would be weaker than the same interaction in boraneamines. In any case, the nature of the C(4)−H(4)....C-(7)c "interaction", if at all real, is not clear at present and further investigations will be carried out to try to clarify this issue. A bond path connects C(7)−H(71) with N(1)d (Figure 5d), thus showing the three centered character[51,57] of the interactions involving H(71). Table 4 shows also that H(71) and H(73) are at distances of O(1)e which are shorter than others corresponding to closed shell interactions, already described, involving the same H atoms. Despite this fact, neither bond paths nor (3,−1) critical points were found between these H atoms and O(1)e, which means that there is no attractive interaction between them.[15,52] This can be explained based on the directional nature of hydrogen bonds, given that the angles C(7)−H(71)...O(1)e and C(7)−H(73)...O(1)e (Table 4) do not favor a link of this kind. The analysis of the topological properties of all the (3,−1) critical points corresponding to nonbonded interactions, exhibited in Table 4, indicates that the strongest bonds are N(1)−H(12)....O(1) and C(6)−H(6)....O(2). Espinosa et al.[58] have found that among all topological properties, λ_3, the positive curvature at the BCP, is the best indicator to characterize and classify H···O intermolecular interactions. The comparison of λ_3 values would indicate that the strongest interaction is the one that builds the polar chains, N(1)−H(12)....O(1), as it was expected on geometrical grounds.

The intermolecular HBs might rule the molecular organization. Therefore, it is worthwhile to further examine them. Figures 6a and 6b show the deformation density maps in the plane of the interaction that gives rise to the chains and that one containing the centrosymmetric dimer, respectively. The polarization of the lone pairs of the O in the directions of the HB can be observed in these pictures. Figure 6a also shows a slight shift of the dipolar density of H(12) toward the nitrogen atom of the nitro group, which will indicate some influence from one of the O(2) lone pairs on H(12). The hydrogen bonds can be even better illustrated by the Laplacian map in the plane defined by the atoms linked by those interactions. This scalar map will show the local concentration of charge associated with the bonds, the deformations of the shell structure of the atoms and the location of the lone pairs[15]. Figure 7a shows a contour map of $\nabla^2\rho$(r) in the plane of H(12) and both oxygen atoms of the nearest molecule within the chain. The figure shows that the shape of the Laplacian between H(12) and O(1)a resembles that of a saddle. The Laplacian is positive between these two atoms (beyond each atom's valence shell charge concentration) and along the direction of the interaction has a minimum at or close to the critical point (The CP is not necessarily on the same plane of the figure), which is a maximum in a direction perpendicular

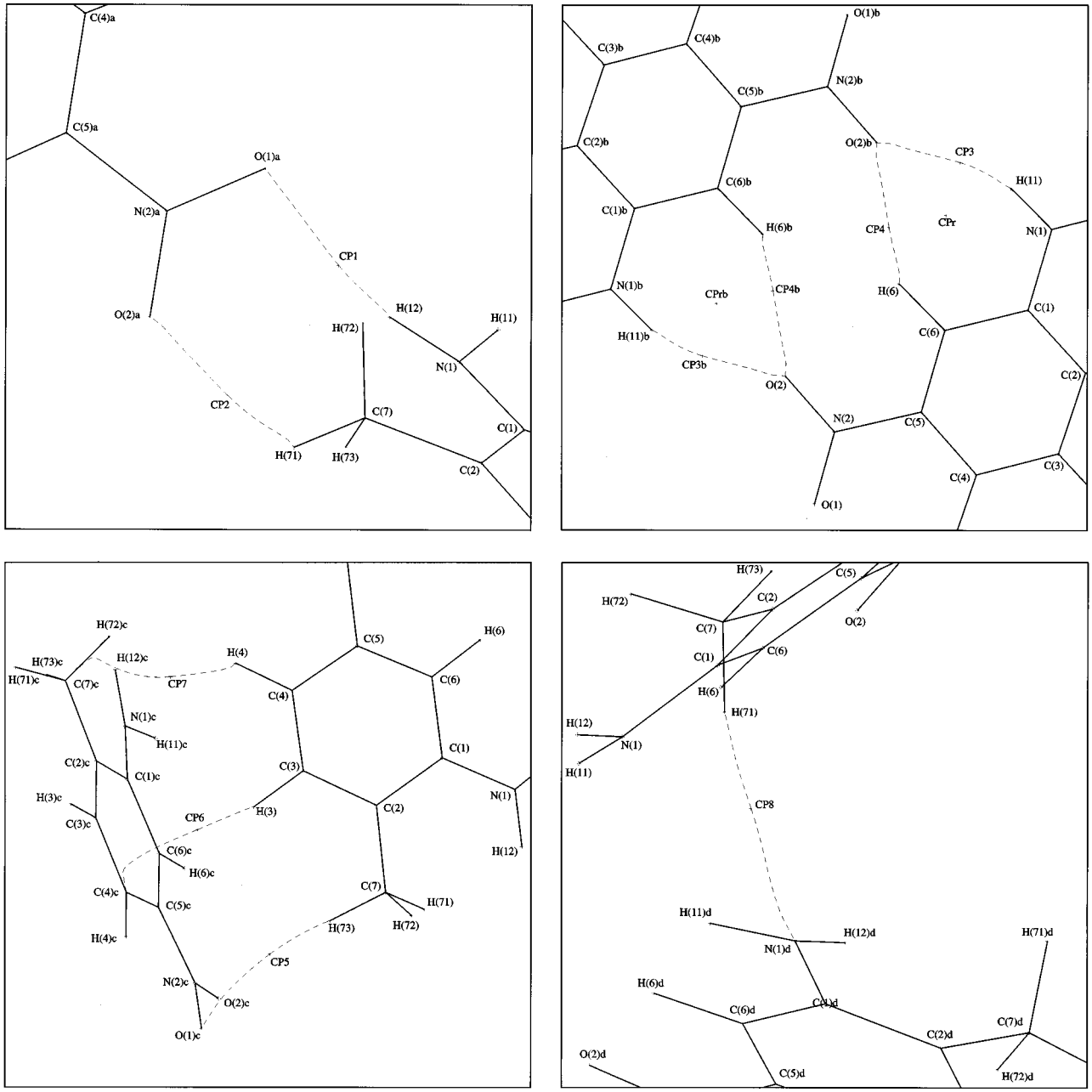

Figure 5. Bond paths for Intermolecular Interactions as detailed in Table 4.

to that of the interaction. The figure also shows that there is not an equivalent feature for the Laplacian along the direction H(12)−O(2)a. This indicates that the N−H···O_{nitro} interaction is, contrary to previous assumptions[5,8], two center. Figure 7b shows a contour map of $\nabla^2\rho(r)$ in the plane of the oxygen O(2) and the hydrogen atoms H(11)b and H(6)b belonging to the other molecule of the centrosymmetric dimer. In this picture, the directionality of the lone pairs of O(2) toward H(11)b and H(6)b can be observed. The contour lines show the same feature explained previously for H(12)−O(1)a, but this time along the directions O(2)−H(11)b, O(2)−H(6)b and their symmetrical equivalents. This agrees with the existence of the N(1)−H(11)...O(2)b and C(6)−H(6)...O(2)b HBs that form the dimer and also with the relative strength of these interactions.

Free Molecule Charge Density. Atomic coordinates and bond distances and angles obtained from the optimization process are deposited as Tables 8S and 9S. Selected conformational parameters of the free and in-crystal 2M5NA molecule are included in Table 5 for comparison. It can be seen from it that the optimized aromatic ring is not planar. However, its total deformation amplitude,[59] Q_T, is smaller than the experimental one. The planarity of the amino group and its coplanarity with the aromatic ring were analyzed, after Ferretti et al.,[60] through the examination of two internal coordinates, τ and χ_N, shown in Scheme 1. These are function of the torsion angles involving the hydrogen atoms: ω_1= C(6)−C(1)−N(1)−H(11), ω_2= C(2)−C(1)−N(1)−H(12); ω_3= C(2)−C(1)−N(1)−H(11) and ω_4= C(6)−C(1)−N(1)−H(12). τ ($0 \le \tau \le 90°$) = $(\omega_1 + \omega_2)/2$, characterizes the rotation around the C(1)−N(1) bond and χ_N ($0 \le \chi_N \le 60°$) = $\omega_2 - \omega_3 + \pi$(mod. 2π) is a measure of the degree of the nitrogen atom pyramidalization (χ_N). The extreme values, 0° and 60°, correspond to a planar sp^2 and a regular tetrahedral sp^3 hybridized nitrogen, respectively. The comparative analysis shows that the optimization predicts for the free molecule a rotation of the amino group around the C(1)−N(1) bond, τ, and a degree of pyramidalization of the aminic nitrogen, χ_N, larger than the experimental ones (see Table 5). Regarding the nitro substituent the calculation results foresee

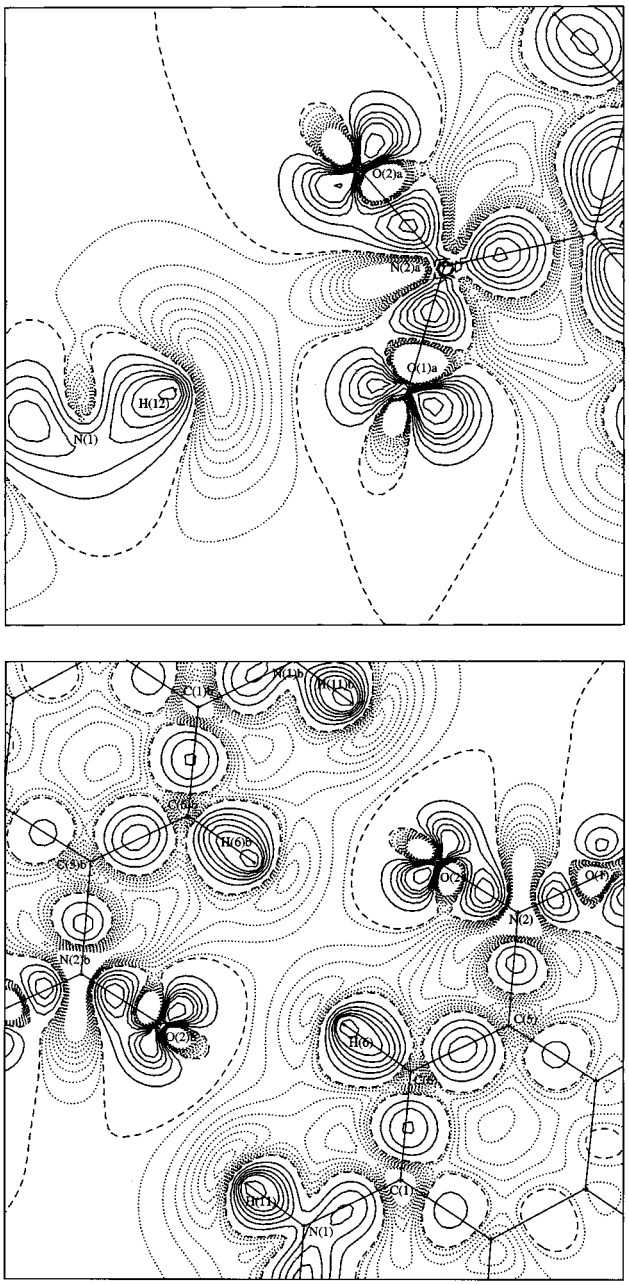

Figure 6. Deformation density maps in the planes of the interactions that give rise to the chains (a) and that form the centrosymmetric dimer (b). Negative contour levels at −0.01, −0.03, −0.05, −0.07, −0.09, −0.11, −0.13, and −0.15 e.Å^{-3} and positive contour levels at 0.1, 0.2, 0.3, 0.4, 0.5, 0.75, 1.0, and 1.25 e.Å^{-3}. Solid contours positive, dashed contour zero and dot contours negative.

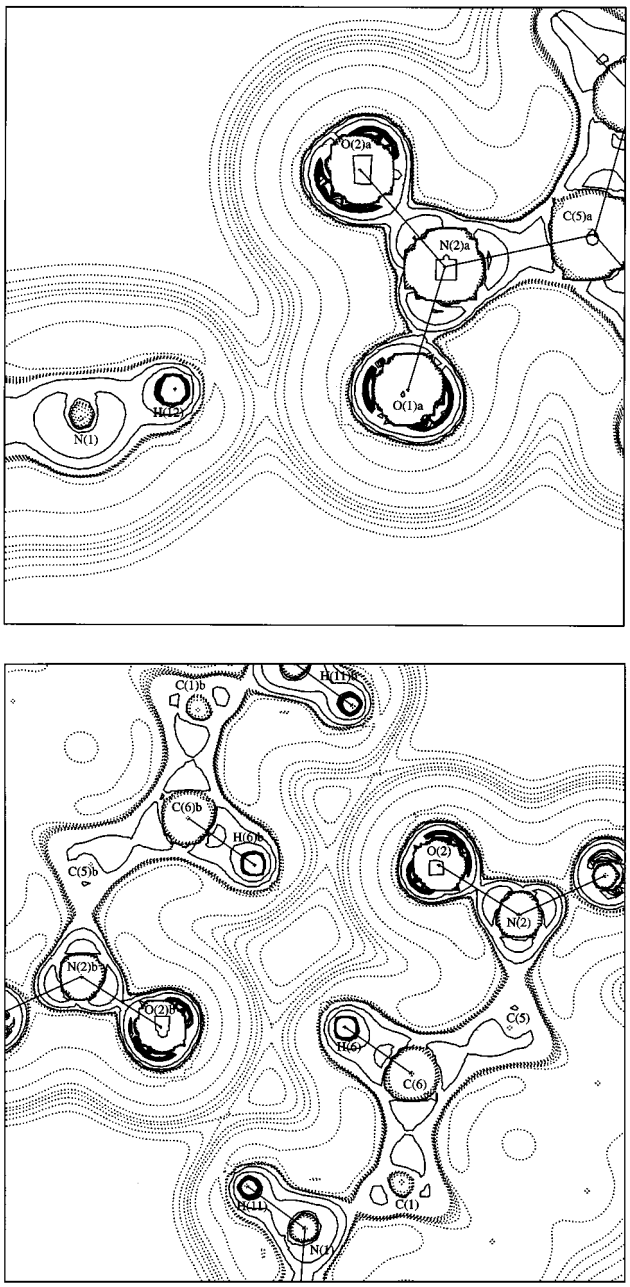

Figure 7. Contour maps of $\nabla^2\rho(r)$ (a) In the plane of H(12), O(1)a and O(2)a. (b) In the plane of O(2), H(6) and O(2)b. Negative contour levels at 5, 20, 60, 70, 80, 90, and 100 e.Å^{-5}. Positive contour levels at 0.5, 0.75, 1.0, 1.25, 1.5, 2.0, 4.0, and 10.0 e.Å^{-5}. Solid contours negative and dot contours positive.

that it must be almost coplanar with the benzene ring. The predicted dihedral angle between the least-squares plane through the ring and the nitro group, Φ-NO_2, is less than 1°, value much smaller that the one found in the crystal, 6.73(6)°.

The comparison of the predicted and experimental bond length values shows that most of them agree, within 0.007 Å, with the ones found in the solid state. The main differences observed, shown in Table 5, are the shortening of the C(1)−N(1), the N−O and N−H bond lengths. The predicted values for the bond angles involving the aminic N are smaller than the experimental ones. This is consistent with the conformational results and indicates that the aggregation induces some degree of planarization of the amino group. The rotation of the nitro group out of the mean ring plane in the crystal can be ascribed to the intermolecular interactions. In turn, the existence of some degree of conjugation along the chains could explain the conformational change of the aminic nitrogen when going from the free molecule to the aggregation state as well as the shortening of the C(1)−N(1) bond distance in the crystal.

The dipolar moment of the free molecule was calculated at two levels of theory, HF and MP2. Both values are similar, 5.97 and 6.39D, in good agreement with the experimental value in solution 6.12(5)D[42] and, accordingly, smaller than the experimental value obtained in the crystal. To establish whether these differences were due to the unlike in-crystal an free molecular geometries, the molecular dipolar moment was recalculated at the experimental molecular geometry. The value obtained, 6.74D, shows only a 10% increase. This indicates that the change in molecular geometry when going from the gas to

TABLE 5: Selected Conformational and Geometrical Parameters from the Experimental and Minimum Energy Conformation Data

	MP2/6-31G*	experimental
	conf. parameters	
Q_T	0.014	0.0230(8)
Φ-NO_2 (°)	0.95	6.72(5)
τ (°)	7.9	2.7(2)
χ_N (°)	−51.4	−26.5(2)
	bond lengths (Å)	
N(1)−C(1)	1.3978	1.3773(3)
N(1)−H(11)	1.0142	1.0013(3)
N(1)−H(12)	1.0149	1.0023(3)
N(2)−O(1)	1.2434	1.2286(5)
N(2)−O(2)	1.2440	1.2277(5)
N(2)−C(5)	1.4674	1.4634(3)
C(6)−H(6)	1.0858	1.0813(2)
	bond angles (°)	
H(11)−N(1)−H(12)	110. 6	116.4(1)
C(1)−N(1)−H(11)	114.6	117.7(1)
C(1)−N(1)−H(12)	113.7	120.7(1)
C(2)−C(1)−C(6)	120.0	119.1(1)
O(1)−N(2)−O(2)	124.4	122.6(1)
C(6)−C(5)−C(4)	122.8	123.2(1)

[a] $\tau = (\omega_1 + \omega_2)/2$, and $\chi_N = \omega_2 - \omega_3 + \pi$ (mod. 2π), where: ω_1: H(12)−N(1)-C(1)−C(2); ω_2 = H(11)−N(1)-C(1)−C(6); ω_3= H(12)−N(1)-C(1)−C(6).

SCHEME 1

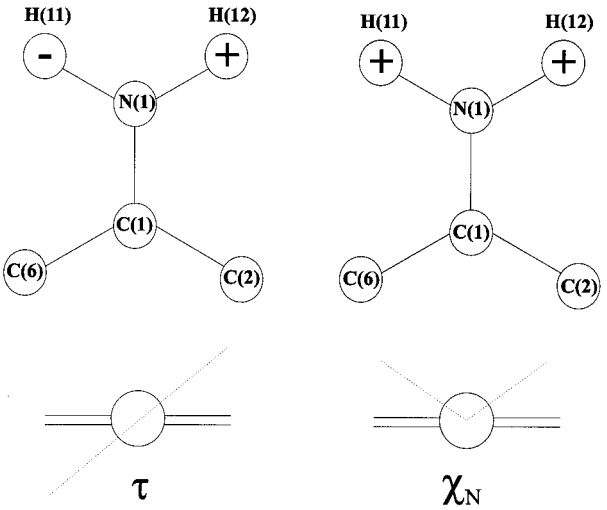

the crystalline phase does not account for the dipolar moment change. Besides, the calculation results allow us to conclude that the molecular dipolar moment in solution is well described by the dipolar moment of the free molecule, whereas, as stated above, the molecular dipolar moment in the crystal is strongly influenced by the crystalline environment.

A topological analysis of the charge density of the free molecule was performed. The search of the (3,−1) BCPs and the properties of the charge density at these points were computed with the program EXTREME.[61] Table 3 shows the values for the bonds of interest. The comparison of the calculated and experimental values pointed that the experimental ellipticities in the C(1)−N(1) and C(5)−N(2) bonds are greater than the calculated ones. This suggests a partially double character of those bonds in the crystal. Besides, the C(1)−N(1) experimental bond charge density at the BCP is larger than the calculated one and the BCP shifts toward N(1) when going from the free molecule to the crystalline state, thus indicating bond polarization. The properties of the charge density at the BCP and the BCP's positions in both N−H bonds of the free molecule are equal. The same is observed at both N−O bonds. The differences observed in the N−H and N−O bonds in the solid state can also be associated to the differences in the intermolecular interactions in which they are involved in the crystal. It should be mentioned that the experimental BCP in the N−O bond of the oxygen atom involved in the intermolecular interaction that gives rise to the chains, N(2)−O(1), is closer to the O than in the other N−O bond, N(2)−O(2). This indicates that the N(2)−O(1) bond has a higher polar character than N(2)−O(2).

Periodic HF Calculation Charge Density. To better assess the influence of the intermolecular interactions on the charge density distribution, a comparison was performed between the electrostatic properties obtained from the multipolar refinement of the experimental X-ray data (i.e., interacting in-crystal molecular densities) and an equivalent refinement of the previously mentioned calculated theoretical structure factors (i.e., noninteracting ab initio molecular electron densities). In this way, we expect the comparison to be valid, as all of the atomic charges and electrostatic properties were obtained using the same method and programs. As for the experimental data, all electrostatic properties of the theoretical molecular charge density distribution were obtained using the program XDPROP. The obtained molecular dipolar moment value, 7.3(1)D, is closer to the free molecule values than to the in-crystal one. The comparison of interacting experimental (IE) and non interacting theoretical (NIT) in-crystal molecular dipole moments shows that intermolecular interactions induce not only an increase in the dipole module but also a rotation of the vector of 7.3° and a slight departure of it from the molecular plane. To go deeper into these results, modifications in atomic electron populations were analyzed.

It is known that the atomic charges are very much dependent on how the atoms are defined. It has been shown that electron-density partitioning, based on aspherical multipole refinements, may be biased by the model[3a]. However, in our case atomic charges for the IE and NIT cases were calculated on the same grounds and so, the observed differences can be attributed to the intermolecular interactions. In accordance with theoretical calculations performed on other systems and found in the literature,[12,19] HBs formation induces changes in the atomic populations. Table 2 shows that all hydrogen atoms in IE molecules have lost electrons when compared with NIT ones. Charge migration to heavy atoms can be related to intermolecular interactions. Koch and Popellier[62] have found that one of the criterions for hydrogen bond formation is loss of charge by the hydrogen atoms. The observed variations in the expansion-contraction parameters of the spherical valence shell and deformation functions are consistent with HBs formation. The increment of all the hydrogen atoms' κ parameter (except for H(3)) indicates contraction when going from NIT to IE. This is in agreement with the expected H atoms volume decrease upon HBs formation.[19,62] Heavy atoms' κ' parameter variations (see Table 2), indicate O(1) and O(2) expansion and N(1) contraction. Analysis of atomic charge modifications upon molecular interactions shows that there is a net flux of approximately 0.15e electrons from the amino to the nitro group and a net flux of 0.52e from the hydrogen atoms to the carbon of the methyl group. It is worth noticing that, although for the NIT case the charges of both aminic hydrogen atoms and both oxygen atoms are alike respectively, differences between the charges of those atoms are found for the IE case. These differences can be related to the diversity of the intermolecular interactions in which they are involved. (see Table 4). Changes are also found in the atomic

dipolar moments, see Tables 4S and 5S, but their contributions only accounts for 10% of the molecular dipolar value modification, whereas the change in that figure when going from the free molecule to the crystalline state is 48%. Therefore, atomic polarization cannot explain the increase in the molecular dipolar moment. This is consistent with theoretical calculations in other systems[12,41]

The topological analysis of the charge density gathers the molecular BCPs and the properties of the charge density at these points shown in Table 3. Comparative examination of the results presented in this table shows that parallel to charge migration, intermolecular interactions induce modifications on the chemical bonds. In IE molecules all the bonds, but N(1)−H(11) and C(2)−C(7), show an increase of the parallel curvature. In the case of the X−H bonds, this finding is concomitant with a shift of the BCP toward the H atom, thus inducing higher polarization The comparison also reveals that the ellipticities of the O(1)−N(1), O(2)−N(1), and C(5)−N(2) bonds are noticeable larger for the IE, indicating an increase in their double bond character upon crystallization. The positions of these bonds' BCPs are shifted toward the nitrogen atoms. A slight increment in the ellipticity of C(1)−N(1) is also observed. No significant differences, within 2σ, are observed in the density values of the IE and NIT at the BCPs except in the O(2)−N(2) BCP where an increase in $\rho(r)$, along with a lower $\nabla^2\rho(r)$, is observed.

Negative regions of electrostatic potential, even those originated by strained C−C bonds are indicators of initial sites for electrophilic attack. Therefore, the relative magnitude of the minimum values of this function can be indicators of the reactivity of those sites toward electrophiles. The knowledge of those minima positions can, then, be used to predict molecular aggregation steps and/or to design fragments suitable for molecular recognition. In the present case, the intermolecular interactions are expected to involve the electrostatic potential negative zones, therefore, the minima of the electrostatic potential of the NIT molecules were found and compared with those of the IE molecules described above. In the NIT molecules the lowest values are close to O(2) and O(1) respectively, as in IE, but their magnitudes are similar, −0.16 e/Å and −0.15 e/Å. A minimum of −0.11 e/Å, not observed in the IE molecules, was found in the lone pair region of N(1). The minima at both sides of the mean aromatic ring plane are alike, −0.07e/Å.

These results seem to indicate that both oxygen atoms are prone to be the leaders in the molecular recognition process. Therefore, the formation of the HB that builds the chain, that is N(1)−H(12)...O(1)a, can be assumed to be the initial point of molecular aggregation. If cooperative effects within the chain helped the interaction, charge redistribution within the nitro and amino groups together with planarization of the latter would be produced by molecular aggregation. This process can also cause the observed disappearance of the electrostatic potential local minimum at the N(1) lone pair.

Further analysis of the differences between the in-crystal and free molecules' geometries, and between experimental and calculated molecular electrostatic properties, indicates that the important molecular charge redistribution caused by the intermolecular interactions, induces first an increase of H(6) acidity and then, the rather strong C(6)−H(6)....O(1) interaction. This, in turn, helps the development of the antiparallel arrangement of the polar chains. In addition, an increase in the intramolecular charge transfer takes place during the molecular aggregation process. It is particularly noticeable the shortening of the C(1)−N(1) bond in the in-crystal molecule compared with the in-vacuum one. The observed differences between IE and NIT molecular electrostatic properties, described above, sustain an enhancement of the molecular conjugation in the crystal. This is although the NIT geometry is coincident with that obtained from the multipolar refinement of the experimental data, which already includes the effects of the environment into the molecular geometry.

Final Remarks

Enhancement of the in-crystal molecular conjugation in hydrogen bonded systems, and resulting electrostatic dipolar moment, has been assigned by different authors to various causes. Crystal field effects[3c], electrostatic interactions between parallel chains[50] and π conjugation through HBs[12] have been claimed to explain the results. Hyper-Rayleigh scattering studies in solution have shown that molecular hyperpolarizability of nitroaniline derivatives can be doubled by HBs, or specific electron donor−acceptor, interactions with solvent.[63] In these systems, no long range order exists. It seems safe, then, to infer that the changes on the molecular properties are induced by the mentioned interactions. It looks feasible to extrapolate this finding to explain our in-crystal results. The planarization of the amino group, the unlike charge rearrangement in both N−O bonds as well as C(1)−N(1) shortening and molecular dipole enhancement despite the antiparallel association of the chains could have been assisted by cooperative effects along the infinite chains in which the 2M5NA molecules organize in the crystal. Our present study strongly points to a model where cooperative effects through relatively weak hydrogen bonds help to build polar chains as the first aggregation mechanism, also increasing molecular conjugation. This model supports Panunto's et al. assumption on chains formation in solution.[5] It would also suggest that in systems where strong HBs are at play, the molecular gas model usually assumed to relate molecular and macroscopic properties might need to be revised. Our model seems to contradict recent calculations performed on *p*-nitroaniline,[3c,3d] based on X-ray molecular charge density, that would indicate that the dominant contribution to crystal binding in this system comes from the dispersion interactions. This apparent discrepancy can be explained by (a) either considering that the molecular recognition and aggregation are driven by long-range interactions, as proposed for chain generation. This process may induce charge redistributions and changes in molecular conjugation that can increase the contribution of terms, other than the electrostatic ones, to the binding energy. (b) Or by considering the possible supramolecular cooperativity of the HB interactions, which was not included when investigating the contribution to dimers' stabilization energy[3c].

Conclusions

The present work shows that the N−H···O interactions giving rise to polar chains formation in nitroanilines may be two-centered, contrary to the three centered model assumed in the literature. The crystallization process induces the partial planarization of the amino group and the enhancement of molecular conjugation. Comparison of the charge density in the free molecule with the solid state one shows a significant molecular charge density redistribution. This mainly affects the donor and acceptor groups involved in the HB along the chains, but also induces a C_{aryl}-H···O HB. The latter helps molecules related by an inversion center and belonging to adjacent chains, to be linked by two intermolecular six membered HB rings involving N−H···O and C_{aryl}-H···O interactions, thus stabilizing the nonpolar ribbons. Parallel ribbons, in turn, interact through C_{aryl}-H...π-electron density of neighboring aromatic rings. The

magnitude of the calculated dipolar moment of the free molecule is almost independent of the geometry and the level of theory used, and agrees with the experimental value in solution. The experimental value strongly increases when passing to the solid state. The redistribution of the molecular charge density and the increase of the dipolar moment when passing from the free molecule to the solid state would indicate the existence of cooperative effects along the chains of 2M5NA and suggest the necessity of new experimental data and calculations in related systems.

Acknowledgment. The authors thank CONICET, UNLP, The British Council and Fundación Antorchas, CICPBA, ANCyPT (PICT 1135) (Argentina), FAPESP (Brazil), CSIC (Spain), and EPSRC (UK) for financial support. G.P. is member of the Carrera del Investigador Científico of CONICET. J.E. thanks FAPESP for a postdoctoral fellowship. J.A.K.H. acknowledges EPSRC for a Senior Research Fellowship. We acknowledge Prof. J. C. Autino for growth of high quality crystals and Prof. P. Coppens and Dr. A. Volkov for provision of the 6-31G** basis set used for the periodic HF calculations. We thank Prof. M. A. Spackman and Dr. D. S. Yufit for helpful discussions.

Supporting Information Available: Tables 1S to 9S as mentioned above are available free of charge via de Internet at http://pubs.acs.org.

References and Notes

(1) See: (a) Bürgi, H; Dunitz, J. D. Eds. *Structural Correlation*. VCH: Weinheim, **1994**. (b) Desiraju, G. R. *Chem. Commun.* **1997**, 1475. (c) Aakeröy, C. B. *Acta Crystallogr. B* **1997**, *53*, 569. (d) Allen, F. K.; Motherwell; W. D. S.; Raithby, P. R.; Shields, G. P.; Taylor, R. *New J. Chem.* **1999**, 25. (e) Motherwell, W. D. S.; Shields, P.; Allen, F. H. *Acta Crystallogr. B* **2000**, *56*, 857, among others.

(2) (a) Krishnamohan Sharma, C. V.; Desiraju, G. R. *J. Chem Soc. Perkin Trans. 2* **1994**, 2345. (b) Sarma, J. A. R. P.; Laxmikanth Rao, J.; Bhanupraskash, K. *Chem. Mater.* **1995**, *7*, 1843 and references therein. (c) Hamada, T. *J. Phys. Chem.* **1996**, *100*, 8777. (d) Turi, L.; Dannenberg J. J. *J. Phys. Chem.* **1996**, *100*, 9638, and references therein.

(3) (a) Volkov, A.; Gatti, C.; Abramov, Y.; Coppens, P. *Acta Crystallogr. A* **2000**, *56*, 252 and references therein; (b) Volkov, A.; Abramov, Y.; Coppens, P.; Gatti, C.; *Acta Crystallogr. A* **2000**, *56*, 332; (c) Abramov, Y. A.; Volkov, A.; Wu, G.; Coppens P. *Acta Crystallogr. A* **2000**, *56*, 585 and references therein; (d) *J. Mol. Struct. (Teochem)* **2000**, *529*, 27.

(4) Bosshhard, Ch.; Sutter, K.; Prête, Ph.; Hulliger, J.; Flörsheimer, M.; Kaatz, P.; Günter, P. *Organic Nonlinear Optical Materials. (Advances in Nonlinear Optics Series, Vol. I)*; Garito A. F., Kajjzar, F. Eds. OPA: Amsterdam, 1995, and references therein.

(5) Panunto, T. W.; Urbánczyk-Lipkowska, Z.; Johnson, R.; Etter, M. C. *J. Am. Chem. Soc.* **1987**, *109*, 7786.

(6) Etter, M. C. *Acc. Chem. Res.* **1990**, *23*, 120.

(7) Ellena, J.; Punte G.; Rivero, B. E. *J. Chem. Cryst.* **1996**, *26(5)*, 319.

(8) Ellena, J.; Goeta, A. E.; Howard, J. A. K.; Wilson, C. C.; Autino J. C.; Punte, G. *Acta Crystallogr. B* **1999**, *55*, 209.

(9) A. E. Goeta, C. C. Wilson, J. C. Autino, J. Ellena & G. Punte. *Chem. Mater.* **2000**, *12*, 3342.

(10) Bludsky, O.; Sponer J.; Leszczynski, J.; Špirko, V.; Hobza P. *J. Chem. Phys.* **1996**, *105*, 11 042.

(11) (a) Isaacs E. D.; Shukla, A.; Platzman, P. M.; Hamann; D. R.; Barbiellini, B.; Tulk, C. A. *Phys. Rev. Lett.* **1999**, *82*, 600. (b) Isaacs E. D.; Shukla, A.; Platzman, P. M.; Hamann, D. R.; Barbiellini, B.; Tulk, C. A. *J. Phys. Chem. Solids* **2000**, *61*, 403.

(12) Gatti, C.; Saunders: V. R.; Roetti, C. *J. Chem. Phys.* **1994**, *101*, 10 686.

(13) Masunov, A.; Dannenberg, J. J. *J. Phys. Chem. A* **1999**, *103*, 178.

(14) Ellena, J. Ph.D. Thesis. Dto. de Física, Fac. de Cs. Exactas Universidad Nacional de La Plata, Argentina, 1998.

(15) Bader, R. F. W. *Atoms in Molecules: A Quantum Theory*; Clarendon Press: Oxford Science Publications: Oxford, 1990.

(16) Lipscomb, G. F.; Garito, A. F.; Narang, R. S. *J. Chem. Phys.* **1981**, *58*, 1509.

(17) Levine, B. F.; Bethea, C. G.; Thurmond, C. D.; Lynch, R. T.; Bernstein, J. L. *J. Appl. Phys.* **1979**, *50*, 2523.

(18) Howard, S. T.; Hursthouse, M. B.; Lehmann, C. W.; Mallinson, P. R.; Frampton, C. S. *J. Chem. Phys.* **1992**, *97*, 5616.

(19) (a) Spackman, M. A.; Byrom, P. G. *Acta Crystallogr. B* **1996**, 1023. (b) Spackman, M. A.; Byrom, P. G.; Alfredsson, M.; Hermansson, K. *Acta Crystallogr. A* **1999**, *55*, 30.

(20) Vries, R. Y. De; Feil, D. Tsirelson, VG. *Acta Cryst B* **2000**, *56*, 118.

(21) Cosier, J.; Glazer, A. M. *J. App. Cryst.* **1986**, *19*, 105.

(22) Kirschbaum, K.; Martin, A.; Pinkerton, A. A. *J. Appl. Crystallogr.* **1997**, *30*, 514.

(23) *SMART. Data Collection Software*, Version 4.05/VMS; Siemens Analytical X-ray Instruments: Madison, Wisconsin, USA, 1996.

(24) *SAINT. Data Reduction Software*, Version 4.05/VMS; Siemens Analytical X-ray Instruments: Madison, Wisconsin, USA, 1996.

(25) Sheldrick, G. M. *SADABS. Empirical Absorption Correction Program*; University of Göttingen: Göttingen, Germany, 1997.

(26) Sheldrick, G. M. XPREP in SHELXTL 5.04/VMS. *An Integrated System for Solving, Refining and Displaying Crystal Structures from Diffraction Data*; Siemens Analytical X-ray Instruments: Madison, Wisconsin, USA, 1995.

(27) Blessing, R. H. *Crystallogr. Rev.* **1987**, *1*, 3.

(28) (a) Coppens, P.; Hall, M. B. Eds. *Electron Distributions and the Chemical Bond*; Plenum Press: New York, USA, **1982**. (b) Coppens, P. *X-ray Charge Densities and Chemical Bonding, International Union of Crystallography*; Oxford University Press: Oxford, UK, **1997**, pp 271.

(29) Hansen, N. K.; Coppens, P. *Acta Crystallogr. A* **1978**, *34*, 909.

(30) Koritsanszky, T.; Howard, S. T.; Su, Z.; Mallinson, P. R.; Richter, T.; Hansen, N. K. *XD. Computer Program Package for Multipole Refinement and Analysis of Electron Density from Diffraction Data*; (Release May 1997), Free University of Berlin: Germany, 1997.

(31) Clementi, E.; Roetti, C. *Atomic Data and Nuclear Data Tables* **1974**, *14*, 177.

(32) (a) Hehre, W. J.; Stewart, R. F.; Pople, J. A. *J. Chem. Phys.* **1969**, *51*, 2657; for a discussion, see also (b) Chen, L.; Craven, B. M. *Acta Crystallogr. B* **1995**, *51*, 1081.

(33) Hirshfeld, F. L. *Acta Crystallogr. A* **1976**, *32*, 239.

(34) (a) Trueblood, K. N.; Goldish, E.; Donohue, J. *Acta Crystallogr.* **1961**, *14*, 1009. (b) Mark, T. C. W.; Trotter, J. *Acta Crystallogr.* **1965**, *18*, 68.

(35) Gopal, R.; Chandler, W. D.; Robertson, B. E. *Can. J. Chem.* **1980**, *58*, 658.

(36) Frisch, M. J.; Trucks, G. W.; Schlegel, H. B.; Gill, P. M. W.; Johnson, B. G.; Robb, M. A.; Cheeseman; J. R.; Keith, T.; Petersson, G. A.; Montgomery, J. A.; Raghavachari, K.; Al-Laham; M. A.; Zakrzewski; V. G.; Ortiz, J. V.; Foresman, J. B.; Peng; C. Y.; Ayala; P. Y.; Chen, W.; Wong, M. W.; Andres, J. L.; Replogle, E. S.; Gomperts, R.; Martin, R. L.; Fox, D. J.; Binkley, J. S.; Defrees, D. J.; Baker, J.; Stewart, J. P.; Head-Gordon, M.; González, C.; Pople, J. A. *GAUSSIAN 94*. Revision B.3. Gaussian, Inc.: Pittsburgh, PA, 1995.

(37) Schlegel, H. B. *J. Comput. Chem.* **1982**, *3(2)*, 214.

(38) Hehre, W. J.; Radom, L.; Schleyer, P. V. R.; Pople, J. A. *Ab Initio Molecular Orbital Theory*; Wiley & Sons: New York, 1986.

(39) Sim, F.; Chin, S.; Dupuis, M.; Rice, J. E. *J. Phys Chem.* **1993**, *97*, 1158.

(40) Saunders, V. R.; Dovesi, R.; Roetti, C.; Causà, M.; Harrison, N. M.; Orlando, R.; Zicivich-Wilson, C. M. *CRYSTAL98 User's Manual*; University of Torino: Italy, 1998.

(41) Platts, J. A.; Howard, S. T. *J. Chem. Phys.* **1996**, *105*, 4668.

(42) Barón, M. Universidad de Buenos Aires, Argentina, Private communication, 1997.

(43) Daniel, C.; Dupuis, M. *Chem. Phys. Lett.* **1990**, *171*, 209.

(44) Masunov, A.; Dannenberg, J. J. *J. Phys. Chem. B* **2000**, *104*, 806.

(45) (a) Zavodnik, V.; Stash, A.; Tsirelson, V.; Vries, R.; Feil, D. *Acta Crystallogr. B* **1999**, *55*, 45. (b) Birkedal, H.; Pattinson, P.; Schwarzenbach, D.; Weber, H. P.; Knudsen K.; Mathiesen, R.; Madsen, D. A Supplement to *Acta Crystallogr. A* **1999**, *55*, 117.

(46) Feil, D. X-ray Diffraction and Charge Density In *The Application of Charge Density Research to Chemistry and Drug Design*; Jeffrey G. A., Piniella, J. F., Eds.; Plenum Press: New York, 1991.

(47) Zhang, Y.; Coppens, P. *Chem Commun.* **1999**, 2425.

(48) Stewart, R. F. Electrostatic Properties of Molecules from Diffraction Data In *The Application of Charge Density Research to Chemistry and Drug Design*; Jeffrey, G. A., Piniella, J. F., Eds.; NATO ASI Series B259, Plenum Press: New York, **1991**.

(49) Su, Z.; Coppens, P. *Acta Crystallogr. A* **1992**, *48*, 188.

(50) Bernstein, J.; Etter, M. C.; Leiserowitz, L. *The Role of Hydrogen Bonding in Molecular Assembling. In Structural Correlation*; Bürgi, H., Dunitz, J. D., Eds.; VCH: Weinheim, **1994**. Vol. 2, p 432.

(51) Jeffrey, G. *An Introduction to Hydrogen Bonding*; Oxford University Press: Oxford. 1997.

(52) Bader, R. F. W. *J. Chem. Phys.* **1998**, *102*, 7314.
(53) Yufit, D. S.; Howard, J. A. K.; Davidson, M. G. *J. Chem. Soc., Perkin Trans. 2* **2000**, 249.
(54) (a) Rozas, I.; Alkorta, I.; Elguero J. *J. Phys. Chem. A* **1997**, *101*, 9457. (b) Tang, T. H.; Cui, Y. P. *Can. J. Chem.* **1996**, *74*, 1162. (c) Novoa, J. J.; Mota, F. *Chem. Phys. Lett.* **2000**, *318*, 345.
(55) Klooster, W. T.; Koetzle, T.; Siegbahn, P. E. M.; Richardson, T. B.; Crabtree, R. H. *J. Am. Chem. Soc.* **1999**, *121*, 6337.
(56) Popelier, P. L. A. *J. Phys. Chem. A* **1998**, *102*, 1873.
(57) Rozas, I.; Alkorta, I.; Elguero J. *J. Phys. Chem. A* **1998**, *102*, 9925.
(58) Espinosa, E.; Souhassou, M.; Lachekar, H.; Lecomte, C. *Acta Crystallogr. B* **1999**, *55*, 563.
(59) Cremer, D.; Pople, J. A.*J. Am. Chem. Soc.* **1975**, *95*, 1354.
(60) Ferretti, V.; Bertolasi, P.; Gilli, P.; Gilli, G.*J. Phys. Chem.* **1993**, *97*, 13568.
(61) Laidig, K. E.; McMaster University, Ontario, Canada, personal communication, 1994.
(62) Koch, U.; Popelier, P. L. A. *J. Phys. Chem.* **1995**, *99*, 9747.
(63) Huyskens, F.; Huyskens, P.; Persoons, J. *J. Phys. Chem.* **1998**, *108*, 8.